TECHNICAL REPORT BRL-TR-3353

BRL

CHARACTERIZATION OF FLOW DISTRIBUTION IN AXISYMMETRIC SHOCK TUBES

STEPHEN J. SCHMIDT
RICHARD J. PEARSON

JUNE 1992

U.S. ARMY LABORATORY COMMAND

BALLISTIC RESEARCH LABORATORY
ABERDEEN PROVING GROUND, MARYLAND

NOTICES

Destroy this report when it is no longer needed. DO NOT return it to the originator.

Additional copies of this report may be obtained from the National Technical Information Service, U.S. Department of Commerce, 5285 Port Royal Road, Springfield, VA 22161.

The findings of this report are not to be construed as an official Department of the Army position, unless so designated by other authorized documents.

The use of trade names or manufacturers' names in this report does not constitute indorsement of any commercial product.

REPORT DOCUMENTATION PAGE

Form Approved
OMB No. 0704-0188

1. AGENCY USE ONLY (Leave blank)	2. REPORT DATE	3. REPORT TYPE AND DATES COVERED
	June 1992	Final, March 1990–April 1992

4. TITLE AND SUBTITLE
Characterization of Flow Distribution in Axisymmetric Shock Tubes

5. FUNDING NUMBERS
WO: 44061-203-63-0003

6. AUTHOR(S)
Stephen J. Schraml and Richard J. Pearson

7. PERFORMING ORGANIZATION NAME(S) AND ADDRESS(ES)
U.S. Army Ballistic Research Laboratory
ATTN: SLCBR-TB-B
Aberdeen Proving Ground, MD 21005-5066

8. PERFORMING ORGANIZATION REPORT NUMBER

9. SPONSORING/MONITORING AGENCY NAME(S) AND ADDRESS(ES)
U.S. Army Ballistic Research Laboratory
ATTN: SLCBR-DD-T
Aberdeen Proving Ground, MD 21005-5066

10. SPONSORING/MONITORING AGENCY REPORT NUMBER
BRL-TR-3353

11. SUPPLEMENTARY NOTES

12a. DISTRIBUTION/AVAILABILITY STATEMENT
Approved for public release; distribution is unlimited.

12b. DISTRIBUTION CODE

13. ABSTRACT *(Maximum 200 words)*

Experiments were conducted to study the characteristics of unsteady flow in a small, axisymmetric shock tube. These experiments have been supplemented by numerical results obtained from the SHARC hydrodynamic computer code. Early SHARC results indicated that a substantial gradient in flow velocity and dynamic pressure may exist along the cross section of the shock tube. To further investigate this phenomenon, additional experiments were performed in which dynamic pressure measurements were made at various radii in the expansion section of the shock tube. Additional calculations with the SHARC code were also performed in which turbulence modeling, artificial viscosity, and second order advection were employed.

The second set of calculations agree very well with the experimental results. These results indicate that the dynamic pressure is nearly constant across the radius of the shock tube. This contradicts the early computational results which were performed with first order advection and without turbulence modeling. As a result of these findings, it was concluded that turbulence modeling was necessary to obtain accurate shock tube flow simulations.

14. SUBJECT TERMS
blast, blast tubes, flow fields, nuclear explosion simulation, nuclear weapons, shock tubes, shock waves

15. NUMBER OF PAGES
47

16. PRICE CODE

17. SECURITY CLASSIFICATION OF REPORT	18. SECURITY CLASSIFICATION OF THIS PAGE	19. SECURITY CLASSIFICATION OF ABSTRACT	20. LIMITATION OF ABSTRACT
UNCLASSIFIED	UNCLASSIFIED	UNCLASSIFIED	SAR

INTENTIONALLY LEFT BLANK.

TABLE OF CONTENTS

INTENTIONALLY LEFT BLANK.

LIST OF FIGURES

INTENTIONALLY LEFT BLANK.

LIST OF TABLES

INTENTIONALLY LEFT BLANK.

ACKNOWLEDGMENTS

The authors wish to acknowledge Paul E. Neumann of Dynamic Science Inc. and James E. Bernhardt of the Ballistic Research Laboratory for their efforts in conducting the experiments and reducing the experimental data.

INTENTIONALLY LEFT BLANK.

1. INTRODUCTION

This report results from work performed by the U.S. Army Ballistic Research Laboratory (BRL) in support of the design of a facility which is intended to subject full scale military equipment to nuclear blast and thermal effects. This facility, described by Pearson *et al.* (1985) is termed the Large Blast/Thermal Simulator (LB/TS) and has been designed to produce a wide range of nuclear blast and thermal environments. Shock overpressures in the simulator can range from $2 - 35$ *psi* and simulated weapon yield can range from $1 - 600$ *kT*.

The LB/TS can be thought of as a large shock tube with a complex geometry. The blast portion of a nuclear blast simulation is accomplished by releasing high pressure gas from a set of relatively small steel driver tubes into a large concrete expansion section. By adjusting the initial driver parameters of pressure, temperature and volume, a desired combination of shock overpressure and simulated weapon yield can be obtained. Adjustments in the area ratio between the driver tubes and the expansion tunnel also affect the blast simulation and are used to extend the facilities operating range.

A simplified 1:57 scale model of the LB/TS was constructed to perform experimental parametric studies of blast simulator performance. This model also served to provide data for computer code validation. The model is a simplified, axisymmetric representation of the more complex LB/TS structure. The flow in the simplified axisymmetric model still contains most of the important features of the flow in the LB/TS. Because the model lacked any thermal radiation simulation capability, it is termed a model of a Large Blast Simulator (LBS) rather than an LB/TS.

The 1:57 scale LBS model is shown in Figure 1. It has a cylindrical driver section of 10.16 *cm* diameter. Attached to the downstream end of the driver is a converging nozzle leading to a 4.80 *cm* throat section which then empties into a cylindrical expansion section which has an inside diameter of 25.40 *cm*.

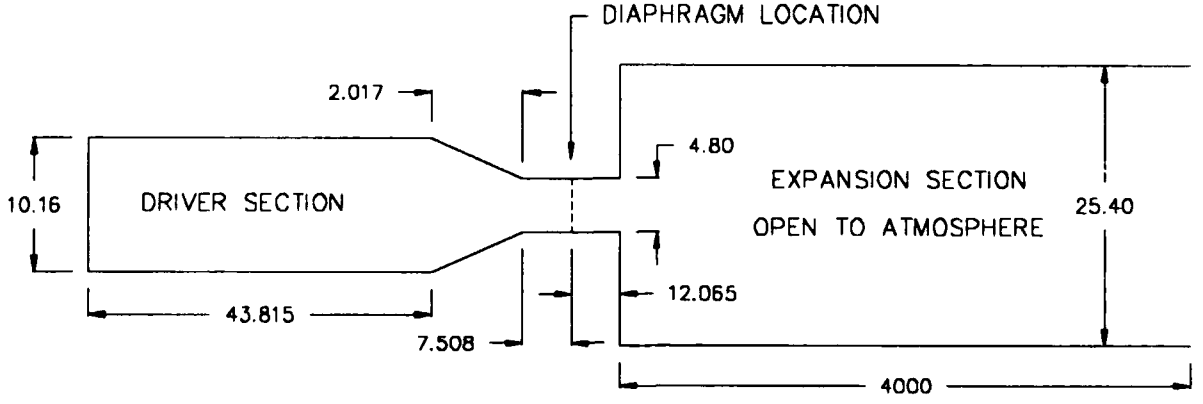

Figure 1. The 1:57 Scale Large Blast Simulator.

Prior to an experiment, the gas in the driver is heated in order to obtain the proper initial conditions for a free field, ideal nuclear blast simulation. One purpose of heating the driver gas is to provide density matching on either side of the contact surface between the gas originally in the driver and the shocked gas, as presented by Opalka (1989). The other purpose of driver gas heating is to add energy to the driver gas which decreases the driver pressure required to produce a given shock overpressure. If the driver gas were not heated, a sudden increase would be seen in the dynamic pressure histories as the contact surface passed the measurement station. Since this phenomenon is not present in the dynamic pressure histories of a free field, exponentially decaying blast wave, it is undesirable in the LB/TS. For this reason, an effort is made to provide contact surface density matching for all 1:57 scale LBS experiments.

2. EXPERIMENTAL MEASUREMENTS

In all the experiments, pressure measurements were taken at a location 177.80 *cm* from the beginning of the expansion section in the axial direction. This axial position corresponds roughly to the center of the test section in the full scale LB/TS. Two pressure gages were employed at this location. A static pressure gage was located with its sensing element flush with the interior surface of the expansion section wall, 12.7 *cm* from the axis of symmetry. A stagnation probe was also positioned at this axial location and was facing upstream into the axial flow. This stagnation gage was mounted in a fixture which could be adjusted to position the face of the gage anywhere along the radius of the circular expansion section.

All the data was recorded using an analog to digital (A/D) card installed in a Zenith model 248 microcomputer. This device can simultaneously record up to 16 channels of data. The maximum sampling rate of the card for one channel is one million samples per second. The maximum sampling rate for 16 A/D channels is 60,000 samples per second. The time and voltage histories for each channel are written to a 12 bit binary disk file by the software which drives the A/D card. These data are then converted to ASCII, after which a data reduction program developed at BRL is then used to derive pressure histories from the pressure gage voltage histories.

By measuring the stagnation and static pressures, the Mach number and dynamic pressure histories can be obtained. Accurate dynamic pressure histories are crucial to blast simulation because it is the dynamic pressure that causes targets to experience large displacements and overturning. In fact, the intended operating envelope of the LB/TS is based on dynamic pressure impulse for shock overpressures above 70 *kPa*.

In order to find the dynamic pressure, one must first determine the Mach number, which can be calculated using the static and stagnation pressures. To obtain the Mach number history, one simply repeats the following set of calculations for each point in the pressure histories. Equation 1 assumes the flow is subsonic and that it is brought to rest at the probe's stagnation point through an isentropic process (Liepmann and Roshko 1957). The

isentropic relation expressed in Equation 1 can be solved for the square of the Mach number yielding Equation 2,

$$\frac{p_0}{p} = \left(1 + \frac{\gamma - 1}{2} M^2\right)^{\frac{\gamma}{\gamma - 1}} \tag{1}$$

$$M^2 = \left(\frac{2}{\gamma - 1}\right) \left[\left(\frac{p_0}{p}\right)^{(\gamma-1)/\gamma} - 1\right] \tag{2}$$

where:

- M is the local Mach number of the gas,
- p_0 is the measured stagnation pressure,
- p is the measured static pressure, and
- γ is the ratio of specific heats (1.400).

If the local Mach number turns out to be greater than 1.0 from Equation 2, then the flow is considered to be supersonic, in which case Equation 3 should be used. Since Equation 3 has no closed form solution for M, a Newton iterative solver is used to determine its value for a given static and stagnation pressure.

$$\frac{p}{p_0} = \left(\frac{2\gamma}{\gamma + 1} M^2 - \frac{\gamma - 1}{\gamma + 1}\right)^{1/(\gamma-1)} \left(\frac{\gamma + 1}{2} M^2\right)^{(-\gamma)/(\gamma-1)} \tag{3}$$

Once the local Mach number is known, the dynamic pressure, q, can be calculated using Equation 4.

$$q = \frac{\gamma}{2} p M^2 \tag{4}$$

3. FLOW DISTRIBUTION INVESTIGATIONS

In an effort to characterize the expected flow patterns in the full scale LB/TS, the Ballistic Research Laboratory conducts a large number of experiments in the 1:57 scale LBS described earlier. A practice employed in many experiments was to position the face of the stagnation probe half way between the centerline and the wall of the expansion section. The probe was positioned to remain above the boundary layer that builds up from the wall after the passage of the shock front. The codes used do not model the boundary layer, so an attempt was made to avoid it in experimental measurements used for comparison. Initially, the probe was not placed on the center line of the expansion tunnel because it is a symmetry boundary in the calculations and the results there are more open to question.

Experimental studies with the 1:57 Scale LBS are often performed in conjunction with computational studies (Opalka and Mark 1986). For one of these studies, the SHARC

hydrodynamic computer code (hydrocode), as described by Hikida *et al.* (1988), was used to simulate the flow in the 1:57 scale LBS and the full scale LB/TS. The SHARC code was chosen over others for this study because of recent improvements which had been made to the code which were thought to be beneficial to this type of calculation. Two of the most important improvements were the addition of an advection scheme which is second order accurate in both time and space and a K-ϵ turbulence model, as presented by Barthel (1985).

Early calculations with the SHARC code were performed using the first order accurate advection scheme without turbulence modeling. The results of these calculations indicated that a large gradient in flow velocity existed along the radius of the axisymmetric shock tube. These results agreed with results that had been previously obtained from the BRL-BLAST2D code, as presented by Hisley (1990).

Liepmann and Roshko (1957) define the dynamic pressure as a function of the square of the velocity in the direction of measurement. It can therefore be concluded that the large axial velocity gradient observed in the initial calculation will likewise create a large dynamic pressure gradient across the radius of the expansion section. It is dynamic pressure which causes targets to experience large displacements and overturning in free field and experimentally simulated blast events. For this reason, accurate computational modeling of dynamic pressure in the full scale LB/TS and the 1:57 scale LBS is crucial to the success of the LB/TS design program. Erroneous dynamic pressure estimates could result in the design of a simulator which is incapable of producing the desired nuclear blast wave simulations.

As a result of the large velocity gradient found in the computational results, an experimental study was initiated to determine if this velocity gradient actually did exist. During the course of the experimentation, the distance from the face of the stagnation pressure gage to the expansion section wall was varied so that a profile of dynamic pressure impulse as a function of radial position could be obtained. The ideal solution would have been to place several gages across the radius of the expansion section. Unfortunately, the size of the gage relative to the diameter of the expansion section prohibited this. The use of multiple gages would have produced a significant blockage of the available flow area in the expansion section, which could result in misleading measurements of dynamic pressure impulse.

In an attempt to improve the comparison between the calculation and experiments, two additional calculations were performed after the tests. In the first calculation, a K-ϵ turbulence model was added and the first order advection scheme used in the initial calculation was retained. In the second calculation, the K-ϵ turbulence model was again used, but a second order advection scheme with artificial viscosity was substituted for the first order advection scheme without artificial viscosity. It has been common practice to employ the artificial viscosity model in all second order advection calculations in order to improve the stability of the code and suppress high frequency oscillations and "overshoots" in the pressure histories. The dynamic pressure histories were obtained by placing a data gathering station in each computational "cell" across the radius of the expansion section 177.80 *cm* downstream from the beginning of the expansion section. This axial position corresponds

exactly to the axial position of the pressure gages in the experiments which allows for direct comparison to the experimental results.

4. RESULTS OF EXPERIMENTS AND CALCULATIONS

An effort was made to keep the initial conditions of all the experiments as close as possible to each another. For each test, the driver overpressure was set at 15.513 *MPa*. The driver temperature was set according to the requirement for density matching across the contact surface as defined by Opalka (1989). This resulted in an average driver temperature of 581.252 *K*. With an average ambient temperature of 285.789 *K*, the ratio of the average driver temperature to the average ambient temperature turns out to be 2.034. The initial conditions for the experiments and the measured dynamic pressure impulse for each test are listed in Table 1.

Table 1. Experimental Results

Station Radius (cm)	Ambient Pressure (kPa)	Ambient Temp. (K)	Driver Temp. (K)	Dynamic Pressure Impulse ($kPa-s$)
0.000	102.87	284.261	578.150	0.711
0.000	102.94	288.150	585.372	0.726
0.000	103.77	284.261	576.483	0.872
3.175	103.22	282.039	573.706	0.722
3.175	102.39	283.706	578.150	0.800
6.350	103.77	284.261	576.483	0.719
9.525	102.73	282.039	573.150	0.643
9.525	102.94	278.706	565.928	0.676
9.525	103.77	291.483	590.928	0.711
9.525	102.25	279.817	570.372	0.745

Standard atmospheric pressure and temperature, 101.325 *kPa* and 288.15 *K* respectively, were employed in the calculations. To match the experiments, the driver overpressure was set to 15.513 *MPa* while the driver temperature used was 585.37 *K*. The driver temperature ratio for the calculations turns out to be 2.031, which compares well with the experimental average of 2.034.

The results of the calculations are summarized in Table 2. At the top of this table is a key for determining which calculation is represented by each column. As the key indicates, the column labeled "M3T0V0" is the first order advection calculation with no turbulence or viscosity. "M3T1V0" represents the first order advection calculation using K-ϵ turbulence and no viscosity. And the label "M4T1V1" stands for second order advection with K-ϵ turbulence and artificial viscosity.

Table 2. Computational Results

M3: First Order Advection M4: Second Order Advection T0: K-ϵ Turbulence Off T1: K-ϵ Turbulence On V0: Artificial Viscosity Off V1: Artificial Viscosity On			
Station Radius (cm)	Dynamic Pressure Impulse ($kPa - s$)		
	M3T0V0	M3T1V0	M4T1V1
0.200	0.322	0.562	0.630
0.600	0.324	0.564	0.631
1.000	0.326	0.567	0.633
1.400	0.330	0.573	0.636
1.800	0.336	0.580	0.640
2.200	0.346	0.589	0.645
2.591	0.362	0.599	0.650
2.974	0.385	0.609	0.655
3.357	0.416	0.612	0.661
3.740	0.458	0.634	0.664
4.123	0.511	0.647	0.672
4.506	0.579	0.660	0.678
4.889	0.660	0.673	0.683
5.281	0.769	0.686	0.688
5.682	0.893	0.698	0.693
6.083	1.031	0.719	0.701
6.885	1.317	0.727	0.705
7.286	1.443	0.733	0.708
7.687	1.527	0.738	0.710
8.088	1.580	0.740	0.712
8.489	1.580	0.741	0.714
8.890	1.519	0.740	0.715
9.291	1.408	0.738	0.716
9.692	1.237	0.735	0.717
10.093	1.042	0.731	0.718
10.494	0.853	0.727	0.718
10.895	0.653	0.722	0.718
11.296	0.492	0.719	0.719
11.697	0.389	0.714	0.719
12.098	0.340	0.711	0.719
12.499	0.316	0.709	0.719

The dynamic pressure impulse results in Tables 1 and 2 are illustrated in Figure 2. In this figure, the dynamic pressure impulse is plotted as a function of the station radius. At the left of the chart, the station radius of 0.0 *cm* represents the centerline. The wall of the expansion section is located at a radius of 12.7 *cm*.

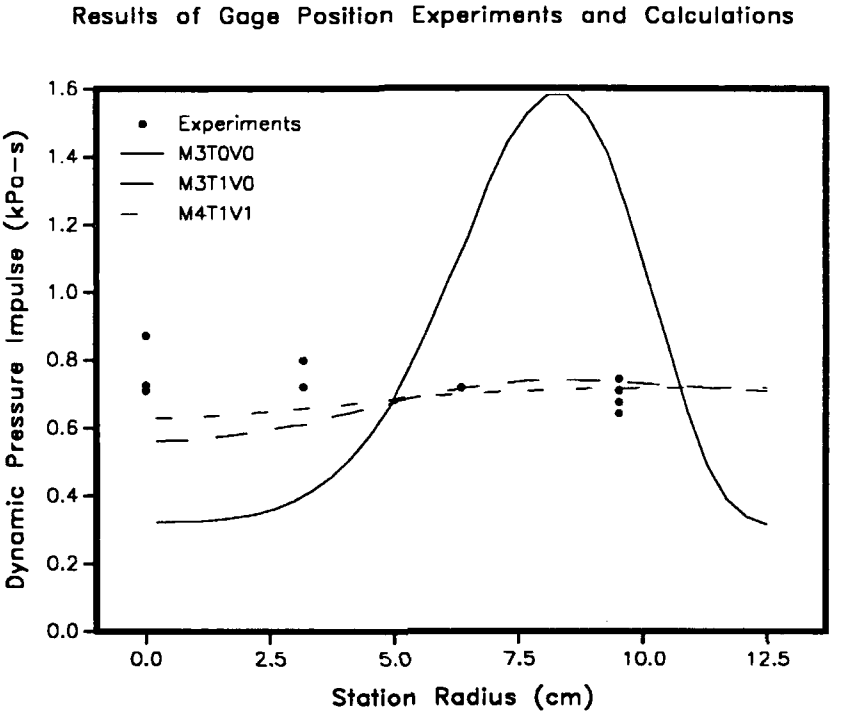

Figure 2. Computational and Experimental Results.

The experimental results are represented by the solid dots. One can see that, according to the experiments, the dynamic pressure impulse is relatively constant across the radius of the expansion section. The experimental impulse is slightly greater at the centerline than it is at the wall. Since the dynamic pressure is a function of the square of the velocity, one would expect this pattern to exist as friction would tend to slow the flow nearest the wall while the flow at the center of the tube would have the greatest velocity.

The three thin lines represent the SHARC computational results. The notation used in the legend of Figure 2 is the same as that in Tables 1 and 2. The solid line shows the results of the calculation using first order advection and no turbulence modeling. This curve illustrates the large gradient in dynamic pressure impulse which initiated the experimental study. The impulse for this calculation is at a minimum at the centerline and then rises to a maximum between 8.0 *cm* and 8.5 *cm*. The minimum impulse at the centerline is well below the experimentally measured impulse at the same location, while the maximum is far greater than the experiments. From this curve, it is evident that a "jet" of high velocity flow persisted between the centerline and the wall, while the flow near the centerline was not nearly as high.

Dynamic pressure histories for this calculation are compared to experiments in Figures 3. 4 and 5. In all cases, the peak dynamic pressure of the "M3T0V0" calculation is greater than the experimentally measured peak. The resulting impulse at the centerline then falls below the experimental history while those at 6.35 *cm* and 9.53 *cm* remain above the experimental dynamic pressure histories. These figures reinforce the result illustrated in Figure 2.

The flow in the expansion section of the BRL 25.4 *cm* shock tube can be further characterized through use of static pressure and Mach number contour plots. Earlier in the report, Equation 4 defined the dynamic pressure as a function of the ration of specific heats, γ, the static pressure, p and the Mach number, M. Since γ is assumed to be constant at 1.4, the dynamic pressure can then only vary with static pressure and Mach number.

The graphics package supplied with the SHARC code is not capable of producing dynamic pressure contour plots, so we must plot both static pressure and Mach number to understand the dynamic pressure patterns in the shock tube. Figures 6, 7 and 8 illustrate the static pressure and Mach number in the shock tube at 10 *ms* for the calculation with first order advection only.

Figure 6 is a static pressure contour plot which is scaled to show the driver section, converging nozzle, throat and the expansion section up to the point where the pressure measurements were taken (2.432 *m*). The pressure range in Figure 6 is from zero to 250 *kPa* with red representing the low pressure and magenta, at the opposite end of the spectrum, representing the highest pressures. Any pressure greater than 250 *kPa* is colored magenta as illustrated by the color of the driver section. The expansion section nearest the top of the plot is the area in which the pressure measurements were taken. The constant, deep blue color of this area indicates that the static pressure here is constant from the centerline to the wall of the expansions section.

Figure 7 is a Mach number contour plot which is drawn to the same scale as Figure 6. The range of Mach numbers in this plot is from 0.0 to 1.0. As in the static pressure contour plot, red represents low values and magenta represents the high end of the spectrum. Contrary to the static pressure profile at the region of interest, a strong Mach number gradient is evident in this plot. To further illustrate this gradient, Figure 8 is provided. This figure is a "close up" view of the expansion section in the region of interest. The experimental and computational pressure measurements were taken at 243.2 *cm* on the vertical axis. Figure 8 demonstrates the cause of the sharp dynamic pressure impulse gradient in the non turbulent calculation. At the centerline (radius=0.0) low Mach number flow exists. Moving from the centerline toward the wall (radius=12.7 *cm*), the Mach number rapidly increases and reaches a maximum at about 8.0 *cm*. From this point outward, the Mach number then rapidly decreases to a very low value at the wall.

After comparing the experimental results to the "M3T0V0" calculation, it became apparent that the large dynamic pressure gradient was most likely an artifact of the calculation. It was determined that in order to improve the distribution of dynamic pressure in the calculations, improved mixing of the flow would be required. As a result, the K-ϵ turbulence model was employed with first order advection in the next calculation, "M3T1V0". The

results of this calculation are illustrated by the long dashed line in Figure 2. One can see that by simply turning on the turbulence model, a tremendous improvement was made to the dynamic pressure impulse distribution as compared to the experimental results. This result still maintained the basic shape of the non turbulent calculation, except at a much reduced scale. The impulse for this calculation was at its minimum at the centerline, maximum at about 8.5 *cm* and then began to drop again near the wall. A look at three specific locations shows that the impulse at the centerline was less than the experimental impulse, while those at 6.35 *cm* and 9.53 *cm* were much closer to the experimentally measured impulse.

Figures 9, 10 and 11 compare dynamic pressure histories from this calculation to experimental histories at the centerline, 6.35 *cm* and 9.53 *cm*. These figures illustrate that calculation "M3T1V0" still over predicts the peak dynamic pressure at all three stations but, in general, is significantly closer to the experimental histories than the non turbulent calculation.

Figures 12, 13 and 14 represent the results of the calculation using first order advection and k-ϵ turbulence modeling. These three contour plots are drawn using the same scales and ranges as Figures 6, 7 and 8 respectively. Figure 12 again illustrates that the static pressure is constant while Figure 13 shows a slight Mach number gradient, though not as strong as in the non turbulent calculation. The "close up" view of the Mach number contours in Figure 14 shows that while some Mach number gradient still exists in the turbulent calculation, this gradient is limited to Mach numbers between 0.3 and 0.4.

A final attempt to improve the computational results was made by using the second order accurate advection scheme along with the K-ϵ turbulence model and the artificial viscosity model. This calculation is referred to as "M4T1V1". Of the three calculations, this one produced the most uniform dynamic pressure impulse. However, while this impulse is nearly uniform, it is interesting to note that the minimum impulse still exists at the centerline, while the maximum impulse exists at the wall.

Dynamic pressure histories from this calculation are compared to experimental histories in Figures 15, 16 and 17. In these figures, one can see that the "M4T1V1" calculation provided a much better match to the experimental dynamic pressure histories than the previous calculations. At the centerline and 6.35 *cm* locations, the peak dynamic pressure nearly matched that of the experiments, while at 9.53 *cm* the calculated peak was slightly higher than the experiment. Overall, the dynamic pressure histories of this calculation closely follow the experimentally measured histories.

Finally, the static pressure and Mach number contour plots for the calculation with second order advection, k-ϵ turbulence and artificial viscosity are shown in Figures 18, 19 and 20. Again, these figures use the same scales and ranges as the previous plots. The results of these plots are very similar to those of the calculation with first order advection and k-ϵ turbulence. The static pressure field in Figure 18 is a constant, deep blue while the Mach number plots of Figures 19 and 20 show a slight gradient with the flow at the centerline slightly lower than the flow near the wall. The "close up" Mach number contour plot of Figure 20 shows that the flow is a little more evenly distributed than that in Figure 14.

These figures demonstrate the significant influence that the k-ϵ turbulence model had on the distribution of flow in the expansion section of the shock tube. Without the turbulence model, strong gradients in flow velocity originating at the beginning of the expansion section, are allowed to persist further downstream. The k-ϵ turbulence model inhibits the propagation of these flow gradients and enhances the mixing in the expansion section resulting in improved agreement with experimental data.

5. CONCLUSIONS

The results of this study indicate that turbulence plays an important role in shaping the flow in the 1:57 scale LBS. The process of flow expansion from the throat section into the expansion tunnel generates a "bottle" shock system. This "bottle" shock system, in turn, creates velocity gradients across the expansion tunnel. When turbulence is not modeled in computer simulations, these flow gradients persist well downstream into the expansion section. These velocity gradients create dynamic pressure gradients which should be measurable in experiments. The experiments, however indicate that these sharp flow gradients do not exist.

Optical studies of flow in blast simulators like the 1:57 scale LBS have been conducted and described by Opalka (1991). These studies demonstrate that this "bottle" shock system is real and that the flow exiting the driver is turbulent. Adding a turbulence model to the computer code greatly improves the agreement with experimental data. It is therefore believed that turbulence plays an important role in shaping the flow in the 1:57 scale LBS and the full scale LB/TS and should be included in numerical simulations of flow in these facilities.

The turbulence model used in these calculations employed a "slip" wall condition which does not model the friction encountered between the fluid and the shock tube walls. Possible future work could involve the use of a turbulence model which takes this friction into consideration. Use of such a model might bring the computational results into closer agreement with the experiments.

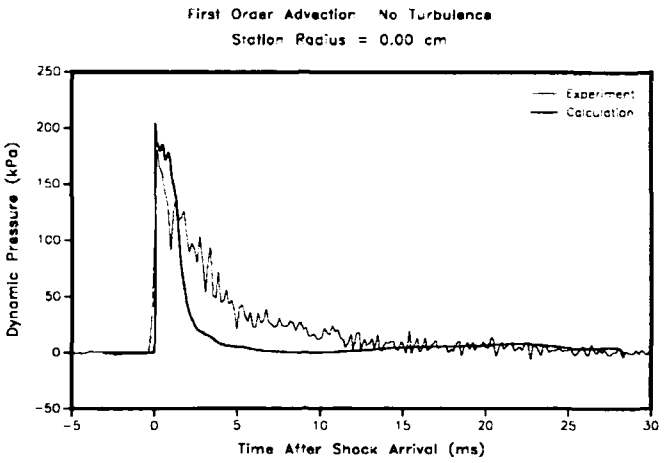

Figure 3. Dynamic Pressure History at 0.00 *cm* for Calculation M3T0V0.

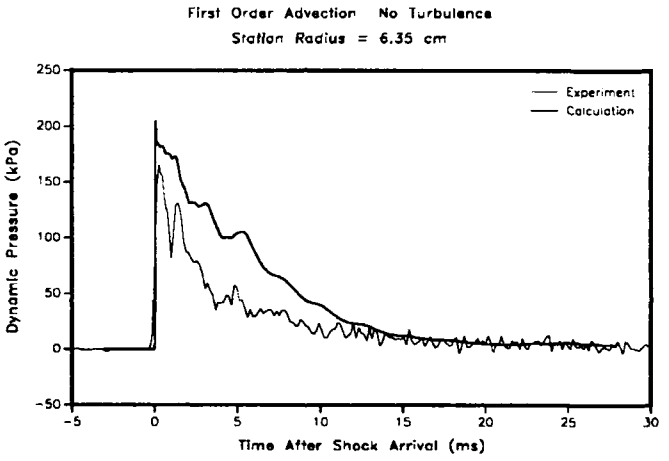

Figure 4. Dynamic Pressure History at 6.35 *cm* for Calculation M3T0V0.

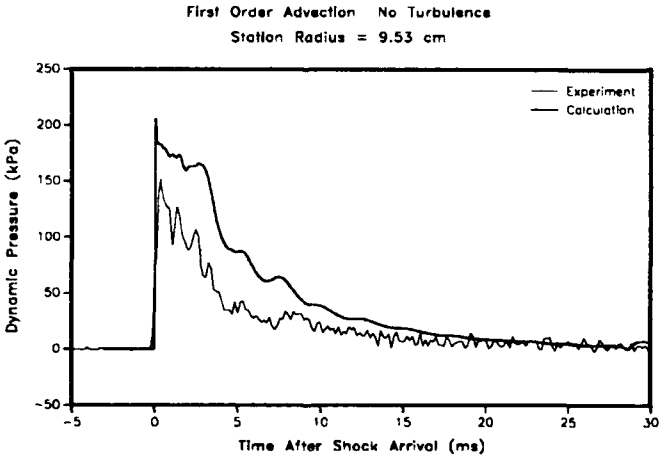

Figure 5. Dynamic Pressure History at 9.53 *cm* for Calculation M3T0V0.

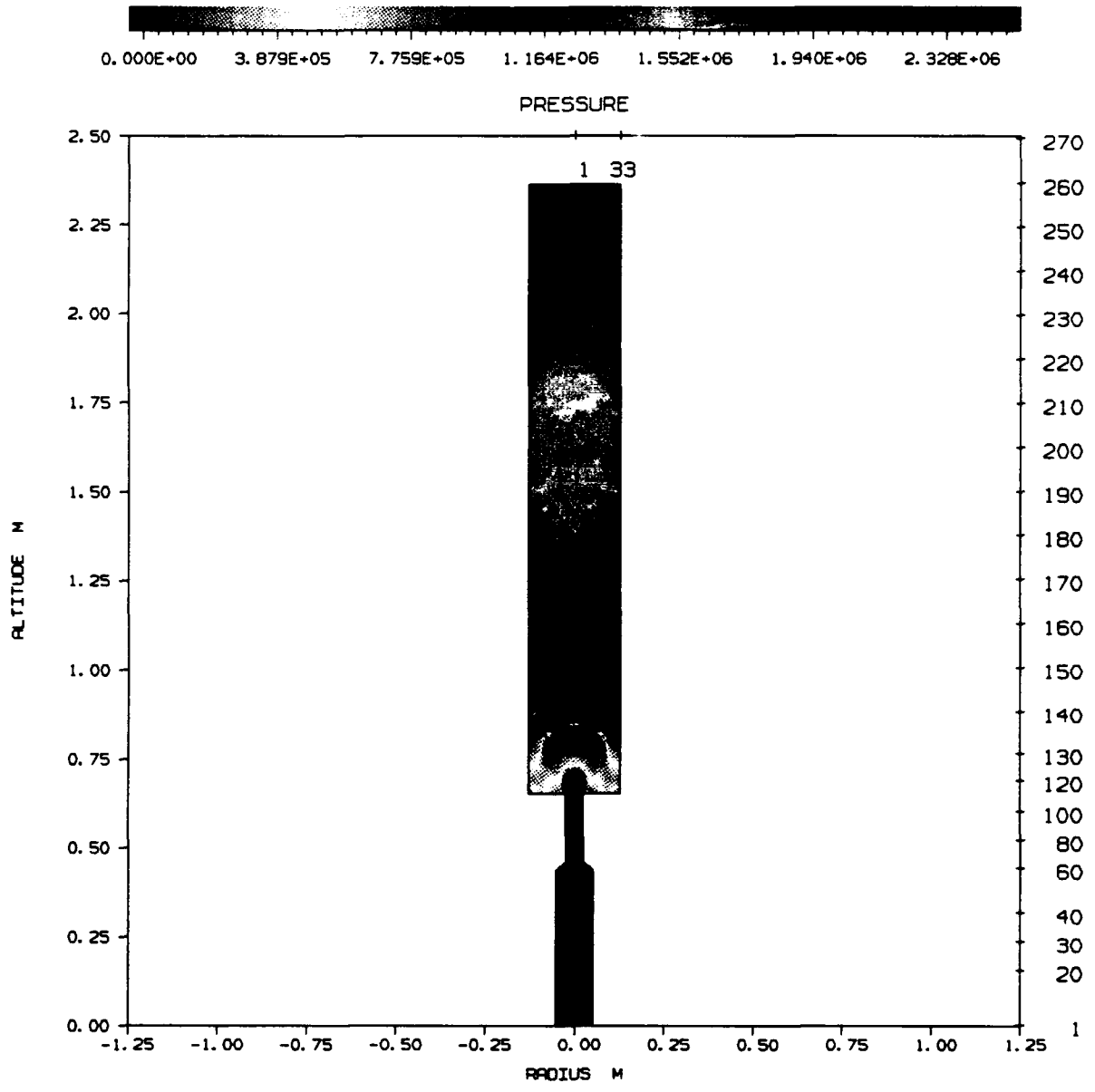

Figure 6. Static Pressure Contours for M3T0V0 Calculation.

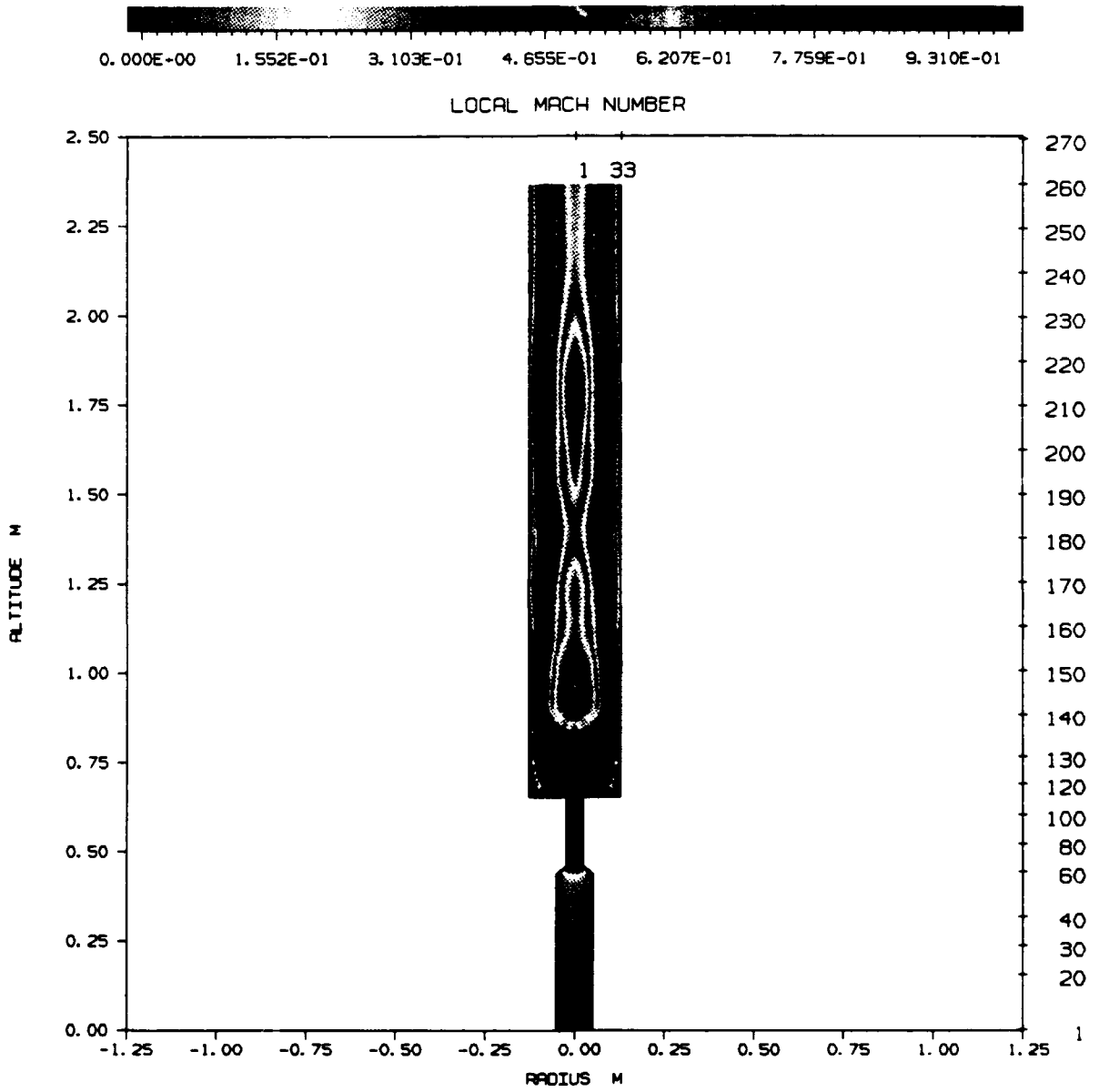

Figure 7. Mach Number Contours for M3T0V0 Calculation.

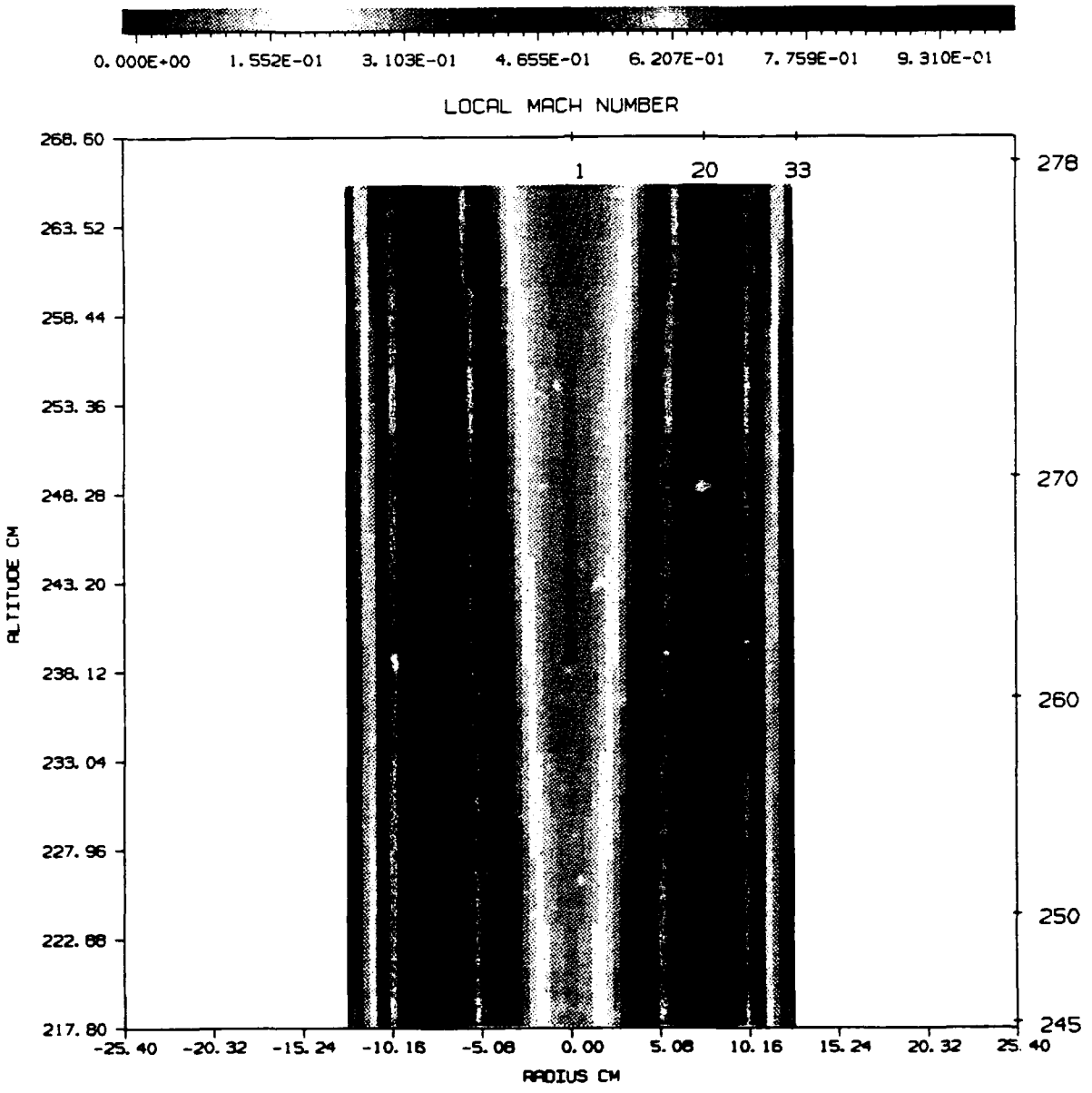

Figure 8. Close Up View of Mach Number Contours for M3T0V0 Calculation.

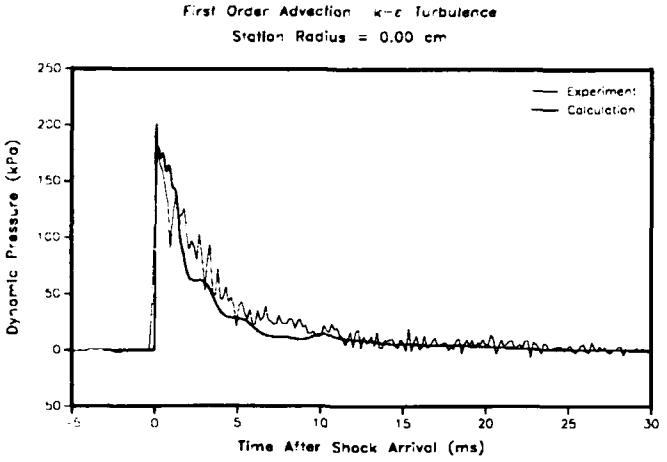

Figure 9. Dynamic Pressure History at 0.00 *cm* for Calculation M3T1V0.

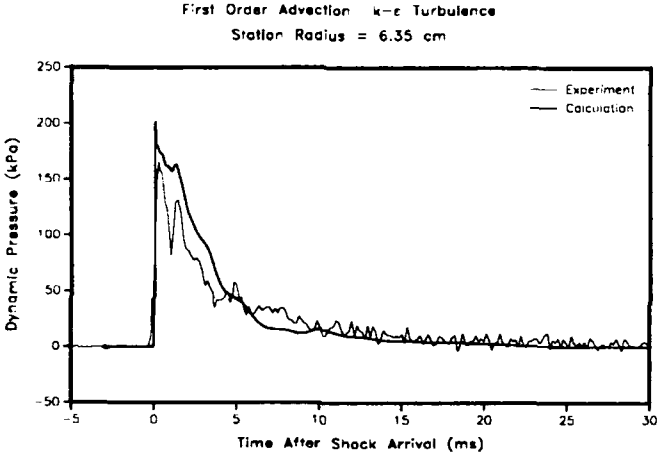

Figure 10. Dynamic Pressure History at 6.35 *cm* for Calculation M3T1V0.

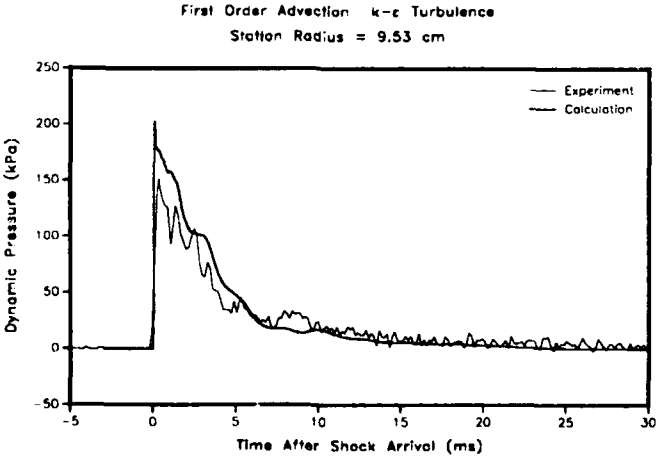

Figure 11. Dynamic Pressure History at 9.53 *cm* for Calculation M3T1V0.

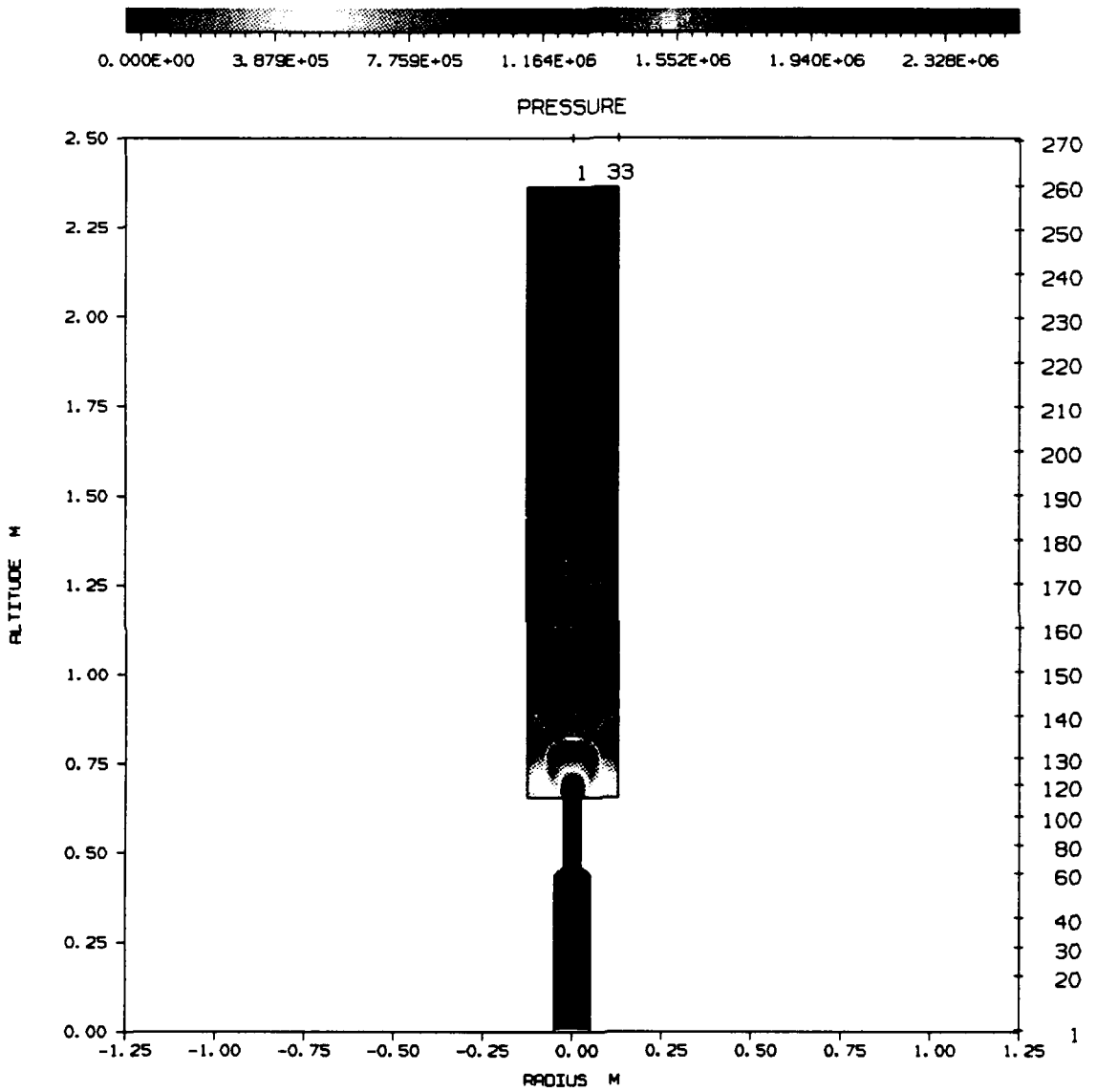

Figure 12. Static Pressure Contours for M3T1V0 Calculation.

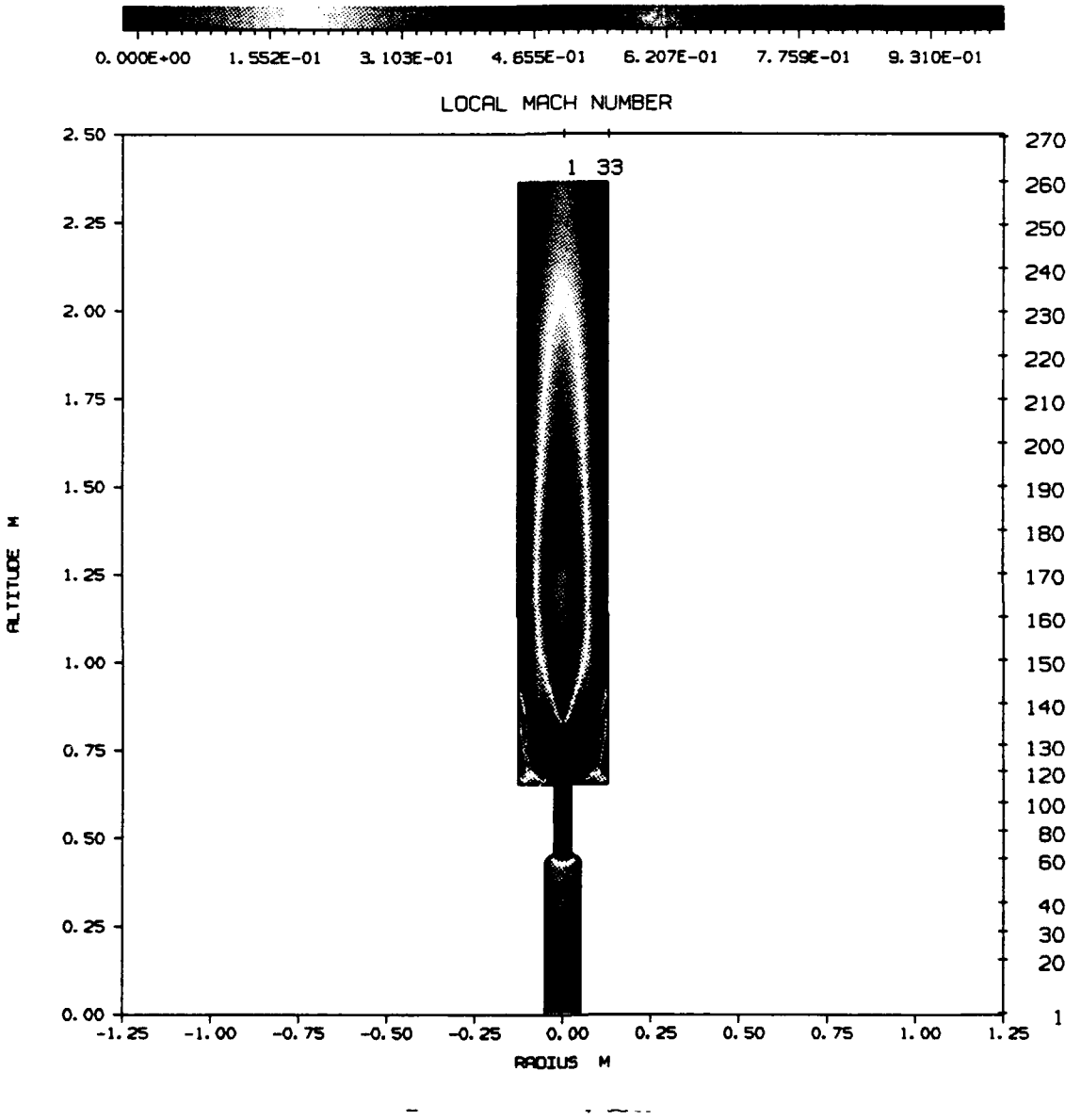

Figure 13. Mach Number Contours for M3T1V0 Calculation.

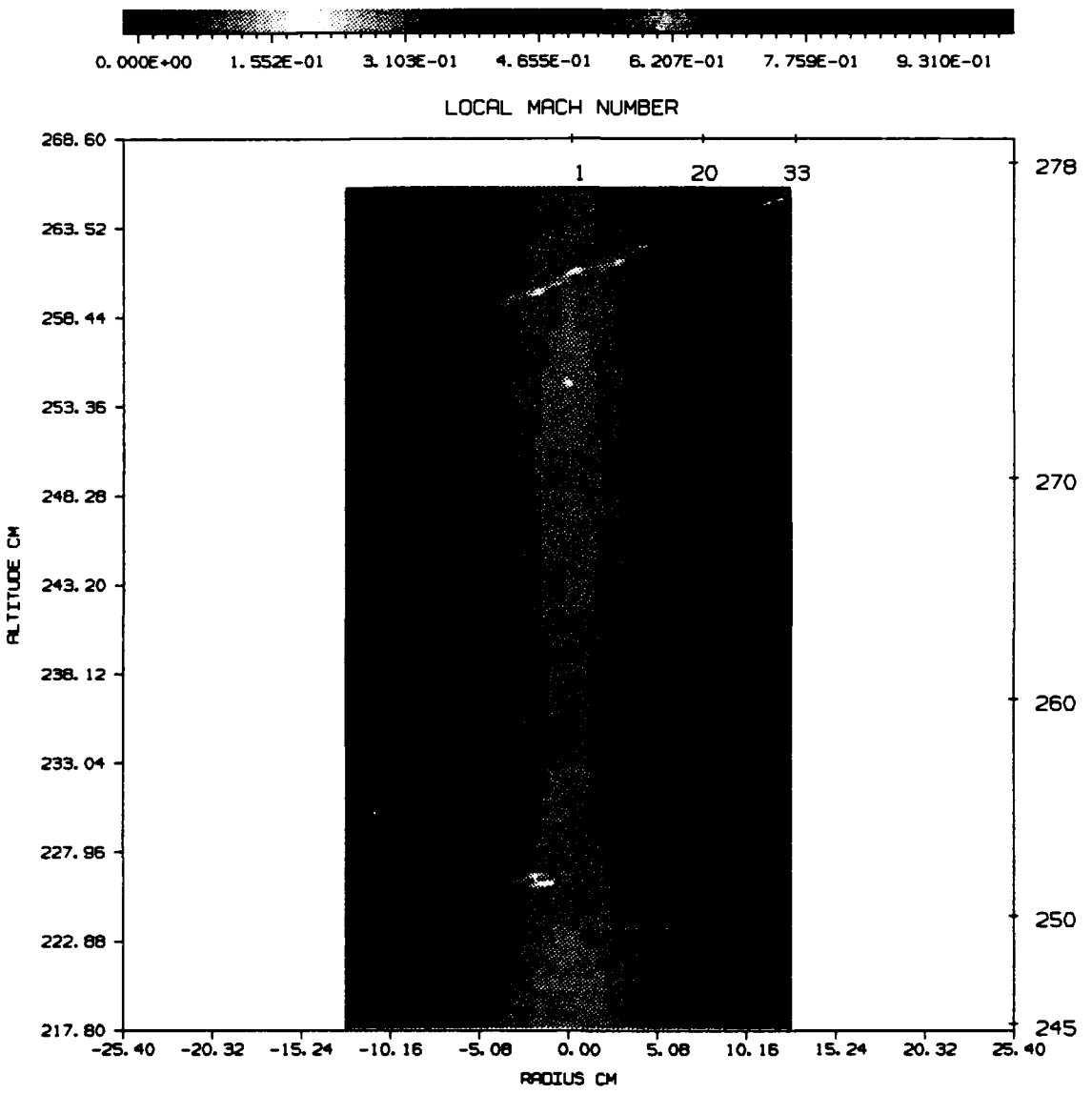

Figure 14. Close Up View of Mach Number Contours for M3T1V0 Calculation.

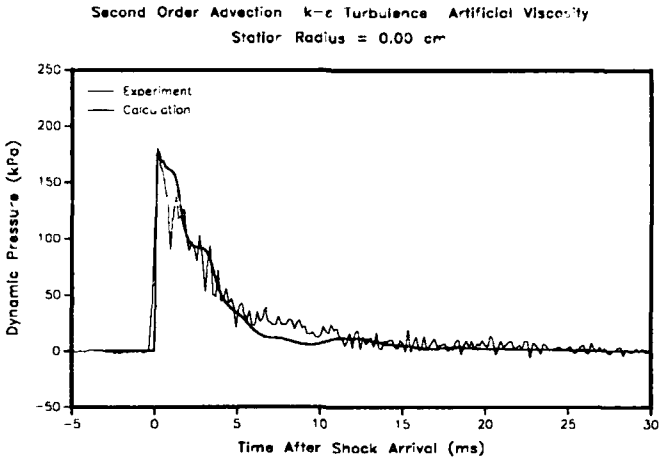

Figure 15. Dynamic Pressure History at 0.00 *cm* for Calculation M4T1V1.

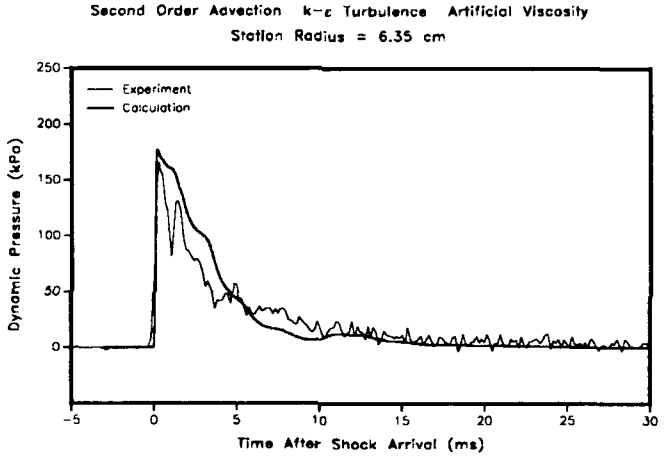

Figure 16. Dynamic Pressure History at 6.35 *cm* for Calculation M4T1V1.

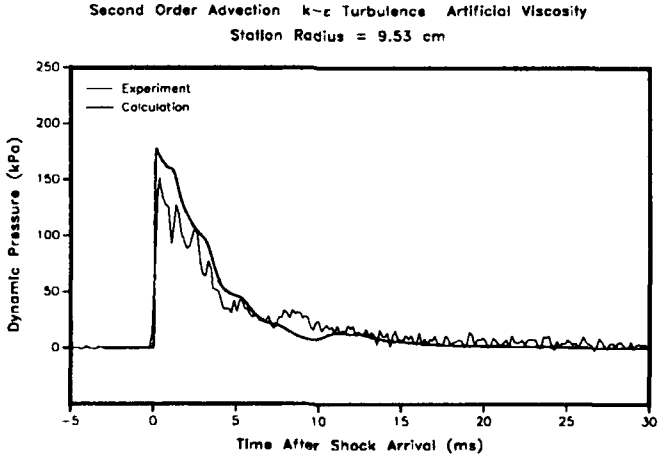

Figure 17. Dynamic Pressure History at 9.53 *cm* for Calculation M4T1V1.

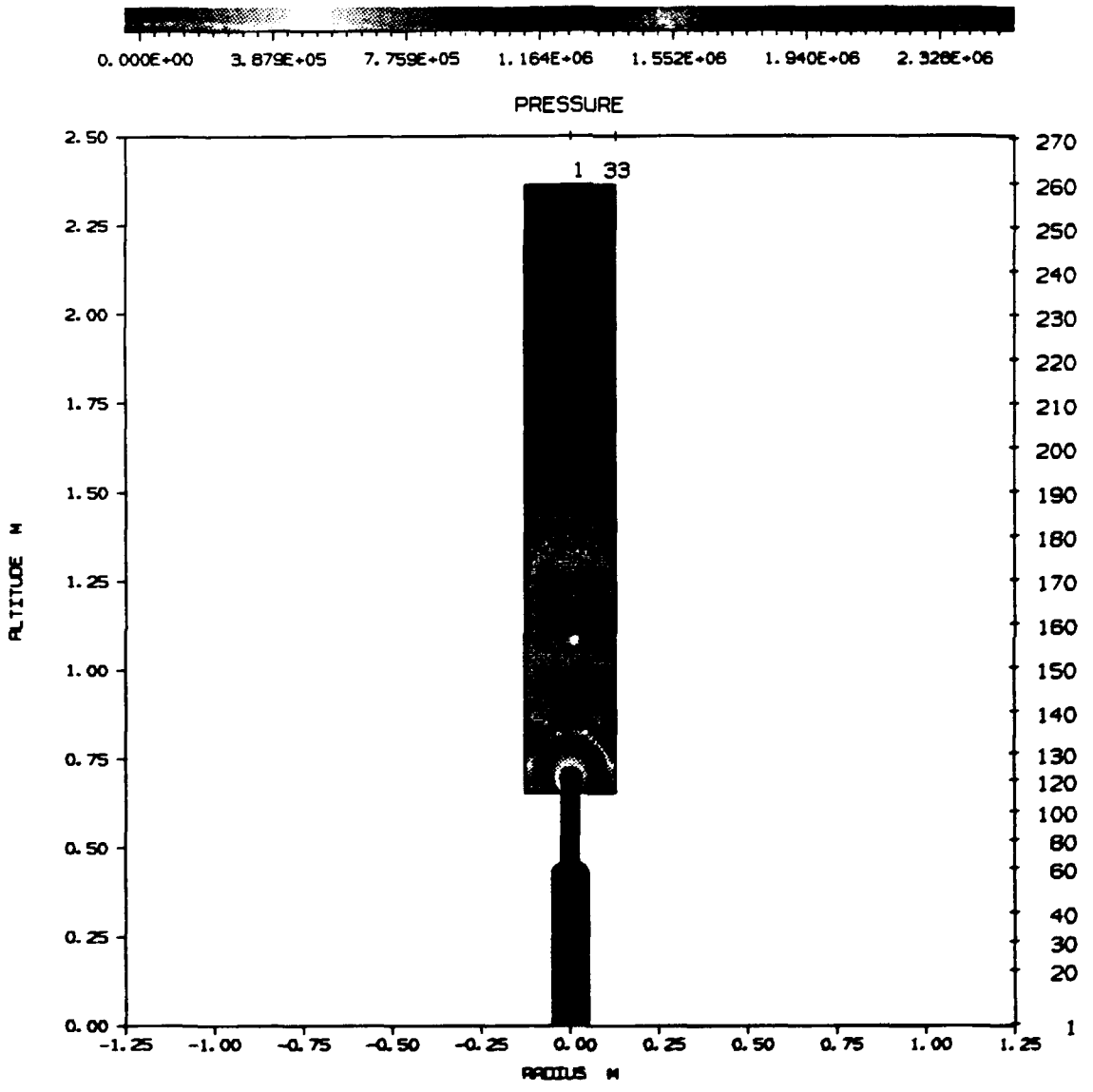

Figure 18. Static Pressure Contours for M4T1V1 Calculation.

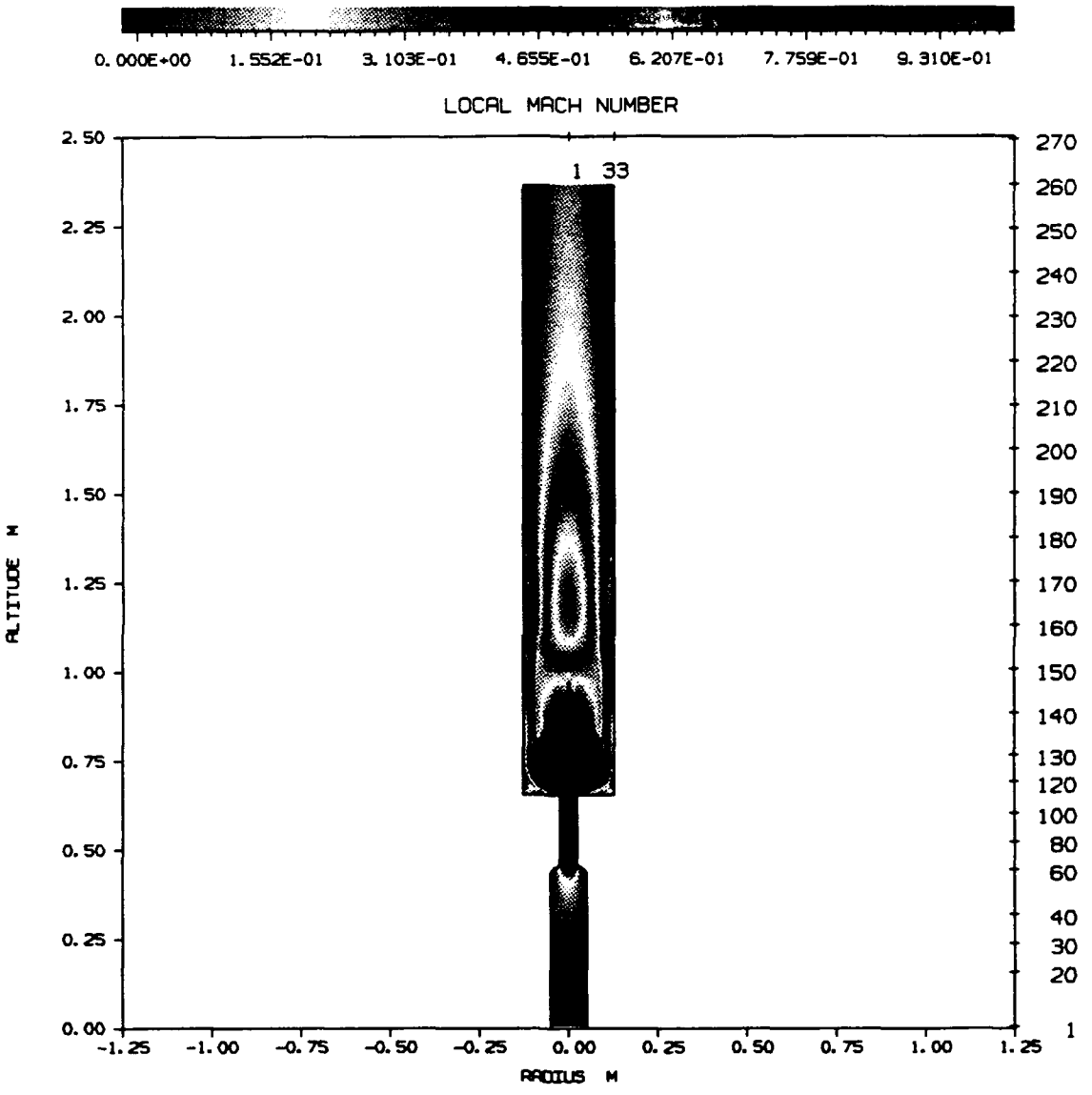

Figure 19. Mach Number Contours for M4T1V1 Calculation.

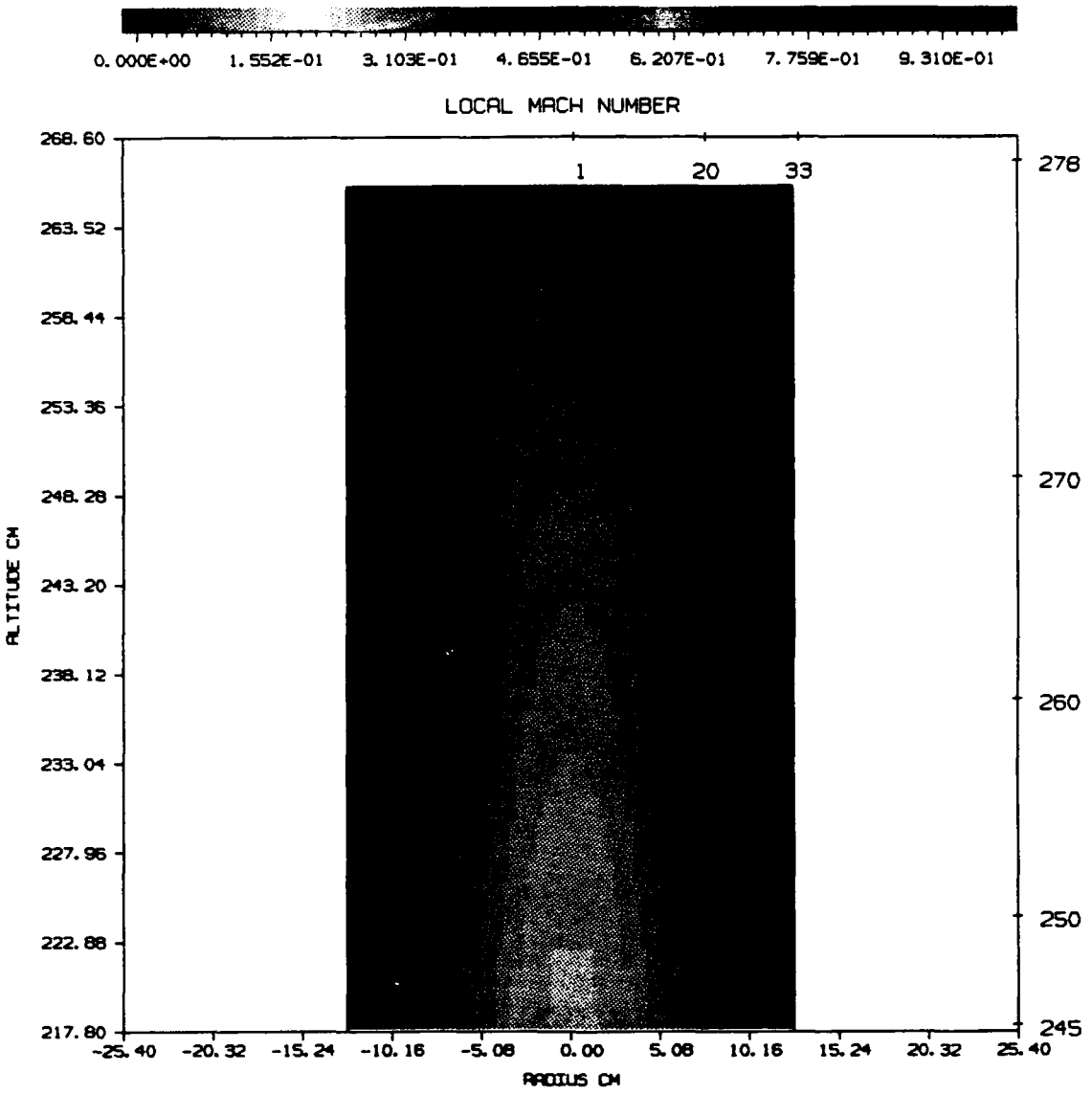

Figure 20. Close Up View of Mach Number Contours for M4T1V1 Calculation.

6. REFERENCES

Barthel, J. "2D Hydrocode Computations Using a K-ϵ Turbulence Model: Model Description and Test Calculations." SSS-TR-85-7115, S-CUBED Technical Report, June 1985, (Footnotes added August 1988).

Hikida, S., R. Bell, and C. Needham. "The SHARC Codes: Documentation and Sample Problems." SSS-R-89-9878, S-CUBED, September 1988.

Hisley, D. "Computational Studies for 1/57-Scale Large Blast Simulator (LBS) Configurations with the BLAST2D Code." BRL-TR-3152, US Army Ballistic Research Laboratory, Aberdeen Proving Ground, Maryland 21005, September 1990.

Liepmann, H., and A. Roshko. "Elements of Gas Dynamics." John Wiley & Sons, Inc., page 148, 1957.

Opalka, K. and A. Mark. "The BRL-Q1D Code: A Tool for the Numerical Simulation of Flows in Shock Tubes with Variable Cross-Sectional Areas." BRL-TR-2763, US Army Ballistic Research Laboratory, Aberdeen Proving Ground, Maryland 21005, October 1986.

Opalka, K. "Large Blast and Thermal Simulator Advanced Concept Driver Design by Computational Fluid Dynamics." BRL-TR-3026, US Army Ballistic Research Laboratory, Aberdeen Proving Ground, Maryland 21005, August 1989.

Opalka, K. "Optical Studies of the Flow Start-Up Process in Four Convergent-Divergent Nozzles Initiated by Bursting a Diaphragm Mounted in the Nozzle Throat." Proceedings of the 12^{th} International Symposium on the Military Applications of Blast Simulation, 22-27 September 1991, Centre d'Etudes de Gramat, 46500 Gramat, France.

Pearson, R., K. Opalka, and D. Hisley. "Design Studies of Drivers for the U.S. Large Blast/Thermal Simulator." Proceedings of the 9^{th} International Symposium on the Military Applications of Blast Simulation, 23-27 September 1985, Atomic Weapons Research Establishment Foulness, Southend-on-Sea, Essex, England SS3 9XE.

INTENTIONALLY LEFT BLANK.

No. of Copies	Organization
2	Administrator Defense Technical Info Center ATTN: DTIC-DDA Cameron Station Alexandria, VA 22304-6145
1	Commander U.S. Army Materiel Command ATTN: AMCAM 5001 Eisenhower Ave. Alexandria, VA 22333-0001
1	Commander U.S. Army Laboratory Command ATTN: AMSLC-DL 2800 Powder Mill Rd. Adelphi, MD 20783-1145
2	Commander U.S. Army Armament Research, Development, and Engineering Center ATTN: SMCAR-IMI-I Picatinny Arsenal, NJ 07806-5000
2	Commander U.S. Army Armament Research, Development, and Engineering Center ATTN: SMCAR-TDC Picatinny Arsenal, NJ 07806-5000
1	Director Benet Weapons Laboratory U.S. Army Armament Research, Development, and Engineering Center ATTN: SMCAR-CCB-TL Watervliet, NY 12189-4050
(Unclass. only) 1	Commander U.S. Army Rock Island Arsenal ATTN: SMCRI-TL/Technical Library Rock Island, IL 61299-5000
1	Director U.S. Army Aviation Research and Technology Activity ATTN: SAVRT-R (Library) M/S 219-3 Ames Research Center Moffett Field, CA 94035-1000
1	Commander U.S. Army Missile Command ATTN: AMSMI-RD-CS-R (DOC) Redstone Arsenal, AL 35898-5010

No. of Copies	Organization
1	Commander U.S. Army Tank-Automotive Command ATTN: ASQNC-TAC-DIT (Technical Information Center) Warren, MI 48397-5000
1	Director U.S. Army TRADOC Analysis Command ATTN: ATRC-WSR White Sands Missile Range, NM 88002-5502
1	Commandant U.S. Army Field Artillery School ATTN: ATSF-CSI Ft. Sill, OK 73503-5000
2	Commandant U.S. Army Infantry School ATTN: ATZB-SC, System Safety Fort Benning, GA 31903-5000
(Class. only) 1	Commandant U.S. Army Infantry School ATTN: ATSH-CD (Security Mgr.) Fort Benning, GA 31905-5660
(Unclass. only) 1	Commandant U.S. Army Infantry School ATTN: ATSH-CD-CSO-OR Fort Benning, GA 31905-5660
1	WL/MNOI Eglin AFB, FL 32542-5000
	Aberdeen Proving Ground
2	Dir, USAMSAA ATTN: AMXSY-D AMXSY-MP, H. Cohen
1	Cdr, USATECOM ATTN: AMSTE-TC
3	Cdr, CRDEC, AMCCOM ATTN: SMCCR-RSP-A SMCCR-MU SMCCR-MSI
1	Dir, VLAMO ATTN: AMSLC-VL-D
10	Dir, USABRL ATTN: SLCBR-DD-T

No of Copies	Organization
1	Director of Defense Research & Engineering ATTN: DD/TWP Washington, DC 20301
1	Assistant Secretary of Defense (Atomic Energy) ATTN: Document Control Washington, DC 20301
1	Chairman Joint Chiefs of Staff ATTN: J-5, R&D Div Washington, DC 20301
2	Deputy Chief of Staff for Operations and Plans ATTN: Technical Library Director of Chemical and Nuclear Operations Department of the Army Washington, DC 20310
1	Director Defense Advanced Research Projects Agency ATTN: Tech Lib 1400 Wilson Boulevard Arlington, VA 22209
2	Director Federal Emergency Management Agency ATTN: Public Relations Office Technical Library Washington, DC 20472
1	Director Defense Intelligence Agency ATTN: DT-2/Wpns & Sys Div Washington, DC 20301
1	Director National Security Agency ATTN: R15, E. F. Butala Ft. George G. Meade, MD 20755
9	Director Defense Nuclear Agency ATTN: CSTI, Tech Lib DDIR DFSP, Ullrich NANS OPNA SPSD, Goering Rohr SPTD, Kennedy Patniak Washington, DC 20305
3	Commander Field Command, DNA ATTN: FCPR FCTMOF NMHE/CDR Lund Kirtland AFB, NM 87115
10	Central Intelligence Agency DIR/DB/Standard ATTN: GE-47 HQ Washington, DC 20505
1	Commandant Interservice Nuclear Weapons School ATTN: Technical Library Kirtland AFB, NM 87115

No of Copies	Organization
4	Director US Army Harry Diamond Labs ATTN: SLCHD-NW-RA, L. Belliveau SLCHD-NW-P, Corrigan Gwaltney SLCHD-TA-L, Tech Lib 2800 Powder Mill Road Adelphi, MD 20783-1197
1	Director US Army Laboratory Command USASMO ATTN: SLCSM-SE, J. Orsega 2800 Powder Mill Road Adelphi, MD 20783-1197
2	Commander, USACECOM ATTN: AMSEL-RD AMSEL-RO-TPPO-P Fort Monmouth, NJ 07703-5301
1	Commander, USACECOM R&D Technical Library ATTN: **ASQNC-ELC-IS-L-R,** Myer Center Fort Monmouth, NJ 07703-5301
1	Director US Army Missile and Space Intelligence Center ATTN: AIAMS-YDL Redstone Arsenal, AL 35898-5500
1	Commander US Army Foreign Science and Technology Center ATTN: Research & Data Branch 220 7th Street, NE. Charlottesville, VA 22901

No of Copies	Organization
1	Director US Army TRAC - Ft. Lee ATTN: ATRC-L, R. Cameron Fort Lee, VA 23801-6140
3	Commander US Army Materials Technology Laboratory ATTN: AMXMR-ATL SLCMT-MEC, W. Haskell SLCMT-MRD-S, K. Ofstedahl Watertown, MA 02172-0001
1	Commander US Army Strategic Defense Command ATTN: CSSD-H-MPL, Tech Lib CSSD-H-XM, Dr. Davies P.O. Box 1500 Huntsville, AL 35807
2	Commander US Army Natick Research and Development Center ATTN: AMDNA-D, Dr. D. Sieling STRNC-UE, J. Calligeros Natick, MA 01762
1	Commander US Army Engineer Division ATTN: HNDED-FD P.O. Box 1500 Huntsville, AL 35807
3	Commander US Army Corps of Engineers Waterways Experiment Station ATTN: CAWES-SS-R, J. Watt CAWES-SE-R, J. Ingram CAWES-TL, Tech Lib P.O. Box 631 Vicksburg, MS 39180-0631

No of Copies	Organization
1	Commander US Army Research Office ATTN: SLCRO-D P.O. Box 12211 Research Triangle Park, NC 27709-2211
3	Commander US Army Nuclear & Chemical Agency ATTN: ACTA-NAW MONA-WE Tech. Lib. 7500 Backlick Rd, Bldg. 2073 Springfield, VA 22150
1	Director HQ, TRADOC RPD ATTN: ATRC-RPR, Mr. Radda Fort Monroe, VA 23651-5143
1	Director TRAC-WSMR ATTN: ATRC-WC, Mr. Kirby White Sands Missile Range, NM 88002-5502
1	Director TRAC-FLVN ATTN: ATRC Fort Leavenworth, KS 66027-5200
1	Commander US Army Test & Evaluation Command Nuclear Effects Laboratory ATTN: STEWS-TE-NO, Dr. J.L. Meason P.O. Box 477 White Sands Missile Range, NM 88002

No of Copies	Organization
2	Chief of Naval Operations ATTN: OP-03EG OP-985F Department of the Navy Washington, DC 20350
1	Director Strategic Systems Projects Office ATTN: NSP-43, Tech Library Department of the Navy Washington, DC 20360
1	Commander Naval Electronic Systems Command ATTN: PME 117-21A Washington, DC 20360
1	Commander Naval Facilities Engineering Command ATTN: Technical Library Washington, DC 20360
1	Commander Naval Sea Systems Command ATTN: Code SEA-62R Department of the Navy Washington, DC 20362-5101
1	Officer-in-Charge Naval Construction Battalion Center Civil Engineering Laboratory ATTN: Tech Lib Port Hueneme, CA 93041
1	Commanding Officer Naval Civil Engineering Laboratory ATTN: Code L51, J. Tancreto Port Hueneme, CA 93043-5003

No of Copies	Organization
1	Commander David Taylor Research Center ATTN: Code 522, Tech Info Ctr Bethesda, MD 20084-5000
1	Commander Naval Surface Warfare Center ATTN: Code DX-21, Library Dahlgren, VA 22448-5000
1	Officer in Charge White Oak Warfare Center Detachment ATTN: Code E232, Tech Library 10901 New Hampshire Ave Silver Spring, MD 20903-5000
1	Commanding Officer White Oak Warfare Center ATTN: Code WA501, NNPO Silver Spring, MD 20902-5000
1	Commander (Code 533) Naval Weapons Center Tech Library China Lake, CA 93555-6001
1	Commander Naval Weapons Evaluation Fac ATTN: Document Control Kirtland AFB, NM 87117
1	Commander Naval Research Laboratory ATTN: Code 2027, Tech Library Washington, DC 20375
1	Superintendent Naval Postgraduate School ATTN: Code 2124, Tech Library Monterey, CA 93940
2	Air Force Armament Laboratory ATTN: AFATL/DOIL AFATL/DLYV Eglin AFB, FL 32542-5000
1	AFESC/RDCS ATTN: Paul Rosengren Tyndall AFB, FL 32403
1	RADC (EMTLD/Docu Library) Griffiss AFB, NY 13441
3	Air Force Weapons Laboratory ATTN: NTE NTED NTES Kirtland AFB, NM 87117-6008
1	AFIT ATTN: Tech Lib, Bldg. 640/B Wright-Patterson AFB, OH 45433
1	FTD/NIIS Wright-Patterson AFB, OH 45433
1	U.S. Department of Energy Idaho Operations Office ATTN: Spec Programs, J. Patton 785 DOE Place Idaho Falls, ID 83402
2	INEL ATTN: Mr. R. Guenzler, MS-3505 Mr. R. Holman, MS-3510 2151 North Blvd., MS-2802 Idaho Falls, ID 83415
1	Director Lawrence Livermore National Laboratory ATTN: Dr. A. Kuhl 5230 Pacific Concourse Dr. Los Angeles, CA 90045

No of Copies	Organization
1	Director Lawrence Livermore Lab. ATTN: Tech Info Dept L-3 P.O. Box 808 Livermore, CA 94550
4	Director Los Alamos National Laboratory ATTN: Mr. Th. Dowler, MS-F602 Dr. J. Chapyak, MS-F664 Doc Control for Reports Library P.O. Box 1663 Los Alamos, NM 87545
3	Director Sandia National Laboratories ATTN: Doc Control 3141 Mr. C. Cameron, Div 6215 Mr. A. Chabai, Div 7112 P.O. Box 5800 Albuquerque, NM 87185-5800
1	Director Sandia National Laboratories Livermore Laboratory ATTN: Doc Control for Tech Library P.O. Box 969 Livermore, CA 94550
1	Director National Aeronautics and Space Administration ATTN: Scientific & Tech Info Fac P.O. Box 8757, BWI Airport Baltimore, MD 21240
1	Director NASA-Langley Research Center ATTN: Tech Lib Hampton, VA 23665
1	Director NASA-Ames Research Center Applied Computational Aerodynamics Branch ATTN: Dr. T. Holtz, MS 202-14 Moffett Field, CA 94035
2	Applied Research Associates, Inc. ATTN: N.H. Ethridge J. Keefer P.O. Box 548 Aberdeen, MD 21001
1	Aerospace Corporation ATTN: Tech Info Services P.O. Box 92957 Los Angeles, CA 90009
1	Agbabian Associates ATTN: M. Agbabian 1111 S. Arroyo Parkway #405 Pasadena, CA 91105-3254
1	Applied Research Associates, Inc. ATTN: R. L. Guice 7114 West Jefferson Ave., Suite 305 Lakewood, CO 80235
1	Black & Veatch Engineers-Architects ATTN: H. D. Laverentz 1500 Meadow Lake Parkway Kansas City, MO 64114
1	The Boeing Company ATTN: Aerospace Library P.O. Box 3707 Seattle, WA 98124
1	California Research & Technology, Inc. ATTN: M. Rosenblatt 20943 Devonshire Street Chatsworth, CA 91311

No of Copies	Organization
1	Carpenter Research Corporation ATTN: H. Jerry Carpenter 27520 Hawthorne Blvd., Suite 263 P.O. Box 2490 Rolling Hills Estates, CA 90274
1	Dynamics Technology, Inc. ATTN: D. T. Hove Suite 300 21311 Hawthorne Blvd. Torrance, CA 90503
1	EATON Corporation Defense Valve & Actuator Div. ATTN: Mr. J. Wada 2338 Alaska Ave. El Segundo, CA 90245-4896
2	FMC Corporation Advanced Systems Center ATTN: Mr. J. Drotleff Ms. C. Krebs, MDP95 2890 De La Cruz Boulevard Box 58123 Santa Clara, CA 95052
1	Goodyear Aerospace Corporation ATTN: R. M. Brown, Bldg 1 Shelter Engineering Litchfield Park, AZ 85340
4	Kaman AviDyne ATTN: Dr. R. Ruetenik (2 cys) Mr. S. Criscione Mr. R. Milligan 83 Second Avenue Northwest Industrial Park Burlington, MA 01830

No of Copies	Organization
3	Kaman Sciences Corporation ATTN: Library P. A. Ellis F. H. Shelton 1500 Garden of the Gods Road Colorado Springs, CO 80907
1	Kaman Sciences Corporation ATTN: Mr. F. W. Balicki 6400 Uptown Boulevard N.E. Suite 300 Albuquerque, NM 87110
1	Ktech Corporation ATTN: Dr. E. Gaffney 901 Pennsylvania Avenue, N.E. Albuquerque, NM 87111
1	Lockheed Missiles & Space Co. ATTN: J. J. Murphy, Dept. 81-11, Bldg. 154 P.O. Box 504 Sunnyvale, CA 94086
2	McDonnell Douglas Astronautics Corporation ATTN: Robert W. Halprin K.A. Heinly 5301 Bolsa Avenue Huntington Beach, CA 92647
1	Orlando Technology, Inc. ATTN: Mr. D. Matuska P.O. Box 855 Shalimar, FL 32579

No of Copies	Organization
2	Physics International Library P.O. Box 5010 San Leandro, CA 94577-0599
2	R&D Associates ATTN: Technical Library Thomas A. Mazzola P.O. Box 9695 Marina Del Rey, CA 90291
1	R&D Associates ATTN: G.P. Ganong P.O. Box 9377 Albuquerque, NM 87119
2	Science Applications, Inc. ATTN: W. Layson John Cockayne P.O. Box 1303 1710 Goodridge Drive McLean, VA 22102
1	Science Applications International Corp. ATTN: Mr. J. Guest 2301 Yale Blvd. SE Suite E Albuquerque, NM 87106
1	Sparta, Inc. Los Angeles Operations ATTN: I. B. Osofsky 3440 Carson Street Torrance, CA 90503
1	Sunburst Recovery, Inc. ATTN: Dr. C. Young P.O. Box 2129 Steamboat Springs, CO 80477
1	Sverdrup Technology, Inc. ATTN: R. F. Starr P.O. Box 884 Tullahoma, TN 37388
3	SRI International ATTN: Dr. G. R. Abrahamson Dr. J. Gran Dr. B. Holmes 333 Ravenswood Avenue Menlo Park, CA 94025
2	S-CUBED A Division of Maxwell Laboratories, Inc. ATTN: C. E. Needham Dr. L. Kennedy 2501 Yale Blvd., SE Albuquerque, NM 87106
3	S-CUBED A Division of Maxwell Laboratories, Inc. ATTN: Technical Library R. Duff K. Pyatt PO Box 1620 La Jolla, CA 92037-1620
1	Texas Engineering Experiment Station ATTN: Dr. D. Anderson 301 Engineering Research Center College Station, TX 77843
1	Thermal Science, Inc. ATTN: R. Feldman 2200 Cassens Dr. St. Louis, MO 63026
1	TRW Ballistic Missile Division ATTN: H. Korman, Mail Station 526/614 P.O. Box 1310 San Bernadino, CA 92402

No of Copies	Organization
1	Battelle ATTN: TACTEC Library, J. N. Higgins 505 King Avenue Columbus, OH 43201
1	California Institute of Technology ATTN: T. J. Ahrens 1201 E. California Blvd. Pasadena, CA 91109
2	Denver Research Institute ATTN: Mr. J. Wisotski Technical Library P.O. Box 10758 Denver, CO 80210
1	Massachusetts Institute of Technology Aeroelastic and Structures Research Laboratory ATTN: Dr. E. A. Witmer Cambridge, MA 02139
1	Massachusetts Institute of Technology ATTN: Technical Library Cambridge, MA 02139
2	New Mexico Engineering Research Institute (CERF) University of New Mexico ATTN: Dr. J. Leigh Dr. R. Newell P.O. Box 25 Albuquerque, NM 87131
1	Northrop University ATTN: Dr. F. B. Safford 5800 W. Arbor Vitae St. Los Angeles, CA 90045
4	Southwest Research Institute ATTN: Dr. W. E. Baker A. B. Wenzel Dr. C. Anderson S. Mullin 6220 Culebra Road San Antonio, TX 78284
1	Stanford University ATTN: Dr. D. Bershader Durand Laboratory Stanford, CA 94305
3	University of Maryland Department of Mechanical Engineering ATTN: Dr. W. Fourney Dr. R. Dick Dr. J. Williams College Park, MD 20742
2	University of Maryland Institute for Advanced Computer Studies ATTN: Dr. L. Davis Mr. G. Sobieski College Park, MD 20742

Aberdeen Proving Ground

1	Cdr, USATECOM ATTN: AMSTE-TE-F, L. Teletski
1	Cdr, USATHMA ATTN: AMXTH-TE

INTENTIONALLY LEFT BLANK.

USER EVALUATION SHEET/CHANGE OF ADDRESS

This laboratory undertakes a continuing effort to improve the quality of the reports it publishes. Your comments/answers below will aid us in our efforts.

1. Does this report satisfy a need? (Comment on purpose, related project, or other area of interest for which the report will be used.) _____

2. How, specifically, is the report being used? (Information source, design data, procedure, source of ideas, etc.) _____

3. Has the information in this report led to any quantitative savings as far as man-hours or dollars saved, operating costs avoided, or efficiencies achieved, etc? If so, please elaborate. _____

4. General Comments. What do you think should be changed to improve future reports? (Indicate changes to organization, technical content, format, etc.) _____

BRL Report Number BRL-TR-3353 Division Symbol _____

Check here if desire to be removed from distribution list. ____

Check here for address change. ____

Current address: Organization _____
Address _____

DEPARTMENT OF THE ARMY
Director
U.S. Army Ballistic Research Laboratory
ATTN: SLCBR-DD-T
Aberdeen Proving Ground, MD 21005-5066

OFFICIAL BUSINESS

BUSINESS REPLY MAIL
FIRST CLASS PERMIT No 0001, APG, MD

Postage will be paid by addressee.

Director
U.S. Army Ballistic Research Laboratory
ATTN: SLCBR-DD-T
Aberdeen Proving Ground, MD 21005-5066

NO POSTAGE
NECESSARY
IF MAILED
IN THE
UNITED STATES